

## Spin correlation measurements for $p$ - $^3\text{He}$ elastic scattering between 4.0 and 10.0 MeV

M. T. Alley\* and L. D. Knutson

*Physics Department, University of Wisconsin, Madison, Wisconsin 53706*

(Received 28 May 1993)

Measurements of the polarization observables for  $^3\text{He}(p,p)^3\text{He}$  elastic scattering have been obtained using a polarized proton beam in conjunction with polarized and unpolarized  $^3\text{He}$  targets. An unpolarized target was used to make high precision measurements of the proton analyzing power  $A_{y0}$  at the energies of 4.01, 5.54, 7.03, 8.52, and 10.01 MeV. A total of 135 data points were obtained with accuracies of typically  $\pm 0.005$  or better. A newly developed polarized  $^3\text{He}$  target was then used to make measurements of the  $^3\text{He}$  analyzing power  $A_{0y}$ , and the spin correlation coefficient  $A_{yy}$  at the same five energies. A total of 48 data points were obtained for each observable. Finally, measurements of the spin correlation coefficients  $A_{xx}$ ,  $A_{zz}$ ,  $A_{zx}$ , and  $A_{xz}$  were made at the single energy of 5.54 MeV. The accuracy of the spin-correlation and  $^3\text{He}$  analyzing power measurements is typically on the order of  $\pm 0.01$ – $0.03$ .

PACS number(s): 24.70.+s, 25.10.+s, 25.40.Cm, 29.25.Pj

### I. INTRODUCTION

Throughout the last thirty years there has been a significant amount of interest in describing  $p$ - $^3\text{He}$  elastic scattering. The various approaches that have been used to reproduce the measurements for this system have included phase shift descriptions [1–3], resonating group calculations [4],  $R$ -matrix analyses [5], cluster model calculations [6], and separable potential models [7]. In view of the theoretical interest in this process, an improved data set including measurements of second-order polarization observables is clearly of value.

Our own interest in  $p$ - $^3\text{He}$  elastic scattering arises in part from the possibility of probing the  $D$ -state components of the  $^3\text{He}$  wave function by using forward dispersion relations [8] to obtain information about the nature of the deuteron exchange amplitudes. For this kind of analysis it is essential to have an accurate set of energy-dependent phase shifts. Prior to our work, phase shift analyses had been hampered by the lack of spin-correlation measurements, which resulted in large phase shift uncertainties and in some cases, multiple phase shift solutions. Because of the difficulties involved in obtaining measurements of second-order polarization observables, there have been only two previous measurements of  $A_{xz}$  and only eight measurements each of  $A_{xx}$  and  $A_{yy}$  in the energy region below 12 MeV [9, 10].

In order to more accurately determine the  $p$ - $^3\text{He}$  phase shifts, we have performed two experiments designed to significantly improve the scattering observable data base. The first experiment has produced high precision measurements of the proton analyzing power  $A_{y0}$ . This was done with a polarized proton beam and a conventional unpolarized  $^3\text{He}$  gas target at the energies of 4.01, 5.54, 7.03, 8.52, and 10.01 MeV. The angular distribution for

each energy consists of 27 points, with errors ranging from 0.0004 to 0.0082. The second experiment involved the use of a newly constructed polarized  $^3\text{He}$  target to measure the spin observables  $A_{y0}$ ,  $A_{0y}$ , and  $A_{yy}$  at the same energies. For these measurements, the angular distribution at each energy consists of 8 to 10 points, with errors ranging from 0.001 to 0.043. Additional measurements of the remaining spin-correlation parameters  $A_{xx}$ ,  $A_{zz}$ ,  $A_{zx}$ , and  $A_{xz}$  (5 points for each observable) were obtained at the single energy of 5.54 MeV.

### II. FORMALISM

We adopt the usual coordinate frame in which the axes  $\hat{x}$ ,  $\hat{y}$ , and  $\hat{z}$  are expressed in terms of the proton initial and final state momenta  $\mathbf{k}_i$  and  $\mathbf{k}_f$  as

$$\hat{z} = \hat{\mathbf{k}}_i, \quad \hat{y} = (\mathbf{k}_i \times \mathbf{k}_f) / |\mathbf{k}_i \times \mathbf{k}_f|, \quad \hat{x} = \hat{y} \times \hat{z}. \quad (1)$$

The convention we use is that the directions of  $\hat{x}$  and  $\hat{y}$  are fixed for scattering to the left-hand side of the beam, which makes  $\hat{y}$  vertical.

In expressing the differential cross section for the experiment, we are interested in the case in which both the initial proton and  $^3\text{He}$  are polarized and final state polarizations are not detected. The azimuthal angle  $\phi$  is defined as the angle between the fixed  $\hat{x}$  axis and the reaction plane. For both of our experiments, the reaction products were detected in the horizontal  $\hat{x}$ - $\hat{z}$  plane, implying that  $\phi = 0^\circ$  or  $180^\circ$ . Following La France [11], the polarized differential cross section for these values of  $\phi$  can be written as

$$\sigma(\theta, \phi) = \sigma_0 \left[ 1 \pm P_{by} A_{y0} \pm P_{ty} A_{0y} \right. \\ \left. + P_{by} P_{ty} A_{yy} + P_{bx} P_{tx} A_{xx} + P_{bz} P_{tz} A_{zz} \right. \\ \left. \pm P_{bx} P_{tz} A_{xz} \pm P_{bz} P_{tx} A_{zx} \right]. \quad (2)$$

\*Present address: Department of Medical Physics, Madison, WI 53706.

The upper sign in Eq. (2) refers to scattering to the left ( $\phi = 0^\circ$ ), while the lower sign refers to scattering to the right ( $\phi = 180^\circ$ ). The proton beam polarization is denoted as  $P_b$ , while the  $^3\text{He}$  target polarization is denoted as  $P_t$ .

### III. UNPOLARIZED TARGET MEASUREMENTS

#### A. Polarized beam

Both of the experiments described in this paper were performed at the University of Wisconsin tandem accelerator laboratory. The polarized proton beam was provided by the Wisconsin colliding beam polarized ion source [12]. The direction of the beam polarization was established with a Wien-filter spin precession magnet which was capable of orienting the polarization vector along any of the three coordinate axes. During the data acquisition the beam current on target was typically 100 nA. After passing through the scattering chamber, the beam entered a polarimeter in which the beam polarization was determined by  $\vec{p}$ - $\alpha$  elastic scattering [13]. The beam polarization was on the order of 0.85 and was statistically determined to 1% over the course of a typical 2 h run. The polarimeter has been calibrated to an accuracy of 2% in the energy range 3–8 MeV, and 1% in the energy range 8–12 MeV. After passing through the polarimeter, the beam was collected in a Faraday cup.

#### B. Target apparatus

Two different scattering cells were utilized for the unpolarized  $^3\text{He}$  measurements. The cells were constructed to cover different angular ranges; the forward angle cell was used in the range of  $20^\circ \leq \theta_{\text{lab}} \leq 65^\circ$ , and the back angle cell used in the range of  $65^\circ \leq \theta_{\text{lab}} \leq 150^\circ$ . The forward angle cell contained a set of internal anti-scattering slits, 2 mm wide by 4 mm high, designed to reduce the background from foil-foil scattering events [14]. The beam entrance and exit openings and the side windows of both cells were covered with  $2.54 \mu\text{m}$  Havar foil. In operation, the cells were attached to the bottom of a liquid nitrogen Dewar designed to fit into the lid of the scattering chamber. During data acquisition the forward angle cell reached a base temperature of typically 150 K, while the back angle cell typically cooled down to 80 K. The forward and back angle cells were operated at 621 and 517 Torr, respectively. In order to reduce the background from possible contaminants in the gas, the cells were filled through a cold trap containing molecular sieve.

Detection of the scattered protons was accomplished with silicon surface barrier detectors mounted 25 cm from the target cell. Measurements were obtained at three different angles simultaneously, using pairs of detectors located symmetrically to the left and right of the beam. The detector slit systems consisted of a forward slit approximately 10 cm from the target and a second slit located directly in front of the detector [14]. Both slits were 1 mm in width, which results in an extreme angular acceptance of  $\pm 0.38^\circ$ . The detectors and slit systems

were mounted on independently movable supports in the scattering chamber. Each support was equipped with a vernier scale which enabled the angular position to be determined to  $0.02^\circ$ .

#### C. Data acquisition and reduction

Measurements were taken in a series of 2 h runs. During each run the beam polarization was reversed every 0.25 s by switching RF transitions at the ion source. Separate spectra were accumulated for the two spin states, and at the end of each run the spectra were recorded on computer disk for later analysis.

The peak of interest was always well isolated in the spectrum, and the background was sufficiently small (well below 1%) that no background subtraction was necessary. A small peak from  $^4\text{He}$  contamination was evident at small angles, but this was well separated from the  $^3\text{He}$  peak.

The electronic dead time was determined by sending pulses to the detector preamplifiers at a rate proportional to the beam current. A typical detector count rate was 5 Hz, and as a consequence all dead times were less than 1%. Dead time corrections to the analyzing power measurements were negligible.

The analyzing power was extracted from the measured peak sums by the usual cross ratio method:

$$A_{y0} = \frac{1}{P_{by}} \left( \frac{X - 1}{X + 1} \right), \quad (3)$$

where

$$X = \left( \frac{L^+ R^-}{L^- R^+} \right)^{\frac{1}{2}}. \quad (4)$$

Here  $L^+$ ,  $L^-$ ,  $R^+$ , and  $R^-$  represent the number of counts in the left and right detectors for the + and - spin states, and  $P_{by}$  is the average beam polarization magnitude.

It was necessary to make corrections to the raw analyzing power measurements to account for energy differences between the data obtained with the forward angle and back angle cells. For the forward angle measurements ( $\theta_{\text{c.m.}} < 83^\circ$ ) the base temperature of the cell was not determined until after the data acquisition runs had been completed. As a result, the proton energies for the forward angle data were systematically higher than those of the back angle measurements by an amount ranging from 320 keV at 4 MeV to 60 keV at 10 MeV. At each of the forward angles, the analyzing power values were corrected to match the energies of the back angle data by performing a polynomial fit of  $A_{y0}$  as a function of energy. The corrections were less than 0.005 at 4 MeV, and less than 0.002 at the remaining energies. The uncertainties in the quoted forward angle analyzing power measurements include estimates of the errors resulting from the polynomial fitting procedure and from the uncertainty in the cell temperature.

The final measurements are listed in Table I. For the back angles the quoted errors consist of statistical uncertainties only, while for the forward angles we include the

TABLE I. Measurements of the proton analyzing power  $A_{y0}$  from the unpolarized  $^3\text{He}$  target. The quoted errors are statistical, except for the forward angles ( $\theta_{c.m.} < 83^\circ$ ) where a contribution arising from the energy adjustment of the data has been included. In addition to the quoted errors, the measurements are subject to an overall scale factor uncertainty of 2% for  $E_p < 8$  MeV and 1% for  $E_p > 8$  MeV.

| 4.01 MeV        |            | 5.54 MeV        |            | 7.03 MeV        |             | 8.52 MeV        |             | 10.01 MeV       |             |
|-----------------|------------|-----------------|------------|-----------------|-------------|-----------------|-------------|-----------------|-------------|
| $\theta_{c.m.}$ | $A_{y0}$   | $\theta_{c.m.}$ | $A_{y0}$   | $\theta_{c.m.}$ | $A_{y0}$    | $\theta_{c.m.}$ | $A_{y0}$    | $\theta_{c.m.}$ | $A_{y0}$    |
| 26.62°          | 0.1105(15) | 26.62°          | 0.0607(12) | 26.63°          | 0.0236(6)   | 26.64°          | 0.0013(5)   | 26.65°          | -0.0113(4)  |
| 33.20°          | 0.1113(17) | 33.21°          | 0.0439(12) | 33.22°          | 0.0038(8)   | 33.23°          | -0.0185(5)  | 33.24°          | -0.0329(7)  |
| 39.70°          | 0.1126(26) | 39.71°          | 0.0337(13) | 39.72°          | -0.0091(8)  | 39.74°          | -0.0348(6)  | 39.75°          | -0.0498(7)  |
| 46.14°          | 0.1164(29) | 46.15°          | 0.0303(14) | 46.16°          | -0.0188(10) | 46.18°          | -0.0475(7)  | 46.19°          | -0.0649(10) |
| 52.47°          | 0.1268(22) | 52.49°          | 0.0341(16) | 52.50°          | -0.0253(10) | 52.51°          | -0.0593(7)  | 52.53°          | -0.0809(6)  |
| 58.74°          | 0.1492(29) | 58.75°          | 0.0431(20) | 58.77°          | -0.0273(14) | 58.78°          | -0.0692(10) | 58.80°          | -0.0942(9)  |
| 64.93°          | 0.1778(32) | 64.94°          | 0.0584(23) | 64.96°          | -0.0242(15) | 64.97°          | -0.0745(11) | 64.99°          | -0.1075(11) |
| 70.98°          | 0.2189(34) | 71.00°          | 0.0849(27) | 71.01°          | -0.0132(20) | 71.03°          | -0.0784(15) | 71.05°          | -0.1180(12) |
| 76.92°          | 0.2630(36) | 76.93°          | 0.1270(31) | 76.95°          | 0.0083(23)  | 76.97°          | -0.0715(16) | 76.98°          | -0.1232(15) |
| 82.72°          | 0.3136(37) | 82.72°          | 0.1848(36) | 82.74°          | 0.0488(28)  | 82.78°          | -0.0486(21) | 82.77°          | -0.1182(18) |
| 88.38°          | 0.3620(63) | 88.39°          | 0.2636(50) | 88.41°          | 0.1146(26)  | 88.43°          | 0.0001(21)  | 88.44°          | -0.0923(17) |
| 93.92°          | 0.3851(66) | 93.94°          | 0.3563(63) | 93.96°          | 0.2174(42)  | 93.97°          | 0.0783(32)  | 93.99°          | -0.0312(17) |
| 99.30°          | 0.4005(68) | 99.32°          | 0.4344(73) | 99.34°          | 0.3403(55)  | 99.35°          | 0.2101(37)  | 99.37°          | 0.0815(23)  |
| 104.53°         | 0.3841(69) | 104.55°         | 0.4871(80) | 104.57°         | 0.4573(74)  | 104.58°         | 0.3721(51)  | 104.60°         | 0.2595(31)  |
| 109.61°         | 0.3647(64) | 109.62°         | 0.4952(82) | 109.64°         | 0.5345(81)  | 109.66°         | 0.5032(54)  | 109.67°         | 0.4606(44)  |
| 114.51°         | 0.3257(58) | 114.53°         | 0.4656(76) | 114.54°         | 0.5477(81)  | 114.56°         | 0.5865(45)  | 114.57°         | 0.5996(51)  |
| 119.28°         | 0.2871(50) | 119.29°         | 0.4206(65) | 119.31°         | 0.5180(76)  | 119.32°         | 0.5851(45)  | 119.57°         | 0.6389(54)  |
| 123.91°         | 0.2486(48) | 123.92°         | 0.3642(62) | 123.94°         | 0.4605(68)  | 123.95°         | 0.5322(41)  | 123.96°         | 0.5921(49)  |
| 128.37°         | 0.2156(41) | 128.39°         | 0.3232(51) | 128.40°         | 0.4014(60)  | 128.41°         | 0.4661(37)  | 128.65°         | 0.5189(44)  |
| 132.70°         | 0.1886(39) | 132.71°         | 0.2776(50) | 132.73°         | 0.3457(53)  | 132.74°         | 0.3974(32)  | 132.75°         | 0.4465(38)  |
| 136.89°         | 0.1660(35) | 136.90°         | 0.2430(40) | 136.91°         | 0.2943(45)  | 136.92°         | 0.3386(28)  | 137.14°         | 0.3737(34)  |
| 140.94°         | 0.1408(36) | 140.95°         | 0.2084(34) | 140.96°         | 0.2551(37)  | 140.97°         | 0.2894(25)  | 141.05°         | 0.3179(36)  |
| 144.88°         | 0.1247(31) | 144.89°         | 0.1845(41) | 144.90°         | 0.2178(40)  | 144.91°         | 0.2434(39)  | 144.92°         | 0.2693(39)  |
| 148.72°         | 0.1047(33) | 148.73°         | 0.1555(28) | 148.74°         | 0.1846(27)  | 148.75°         | 0.2092(19)  | 148.83°         | 0.2242(28)  |
| 152.46°         | 0.0927(29) | 152.46°         | 0.1319(32) | 152.47°         | 0.1560(31)  | 152.48°         | 0.1759(33)  | 152.49°         | 0.1917(31)  |
| 156.10°         | 0.0768(33) | 156.11°         | 0.1099(23) | 156.11°         | 0.1322(20)  | 156.12°         | 0.1468(15)  | 156.19°         | 0.1576(23)  |
| 159.66°         | 0.0666(26) | 159.67°         | 0.0929(30) | 159.68°         | 0.1059(24)  | 159.68°         | 0.1212(26)  | 159.69°         | 0.1323(25)  |

errors from the energy shift as well. In addition to the quoted error there is an overall normalization uncertainty of 1% to 2% resulting from the polarimeter calibration uncertainty. The listed scattering angles have been corrected for a small intrinsic misalignment of the detector slit systems. The uncertainty in  $\theta_{c.m.}$  for each point is estimated to be  $\pm 0.05^\circ$ . The uncertainty in the quoted proton energy for each complete angular distribution is estimated to be  $\pm 0.03$  MeV.

#### IV. POLARIZED TARGET MEASUREMENTS

##### A. The polarized target apparatus

The University of Wisconsin polarized  $^3\text{He}$  target is a low pressure, double-cell system similar in design to the target of Milner *et al.* [15]. The polarization mechanism, which has been previously described by Colegrove *et al.* [16], works as follows. An optical pumping source provides circularly polarized light that is directed upon a weak  $^3\text{He}$  discharge. The polarized light at the wavelength of 1.083  $\mu\text{m}$  produces transitions from the  $2^3S_1$  metastable levels to the  $2^3P$  levels. These states then decay back to the  $2^3S_1$  state, with selection rules  $\Delta L = 1, \Delta m = \pm 1, 0$ . This process alters the magnetic substate population of the metastable atoms, leaving the sample with a net electronic polarization which is then passed on to the nucleus through the hyperfine interaction. The polarization is then transferred to the ground-state atoms through “metastability-exchange collisions,” in which the electron clouds of a polarized metastable atom and an unpolarized ground state atom are interchanged.

As the optical pumping source, we have used a commercial CW YAG laser cavity (Lee Laser model 750M)

with an LNA rod ( $\text{La}_{1-x}\text{Nd}_x\text{MgAl}_{11}\text{O}_{19}$ ) as the lasing medium [17]. The laser was tuned to the 1.083  $\mu\text{m}$   $^3\text{He}$  transition through the use of a single, 0.2 mm uncoated etalon. The pumping power was typically on the order of 1 watt on the helium transition. The circular polarization of the laser, and hence the polarization state of the target, was changed through the use of a rotating quarter-wave plate attached to a stepper motor. This assembly was mounted on the laser rail and was interfaced to a computer so that the target polarization could be automatically changed. Further details are given in Ref. [18].

The  $^3\text{He}$  gas was contained in a double-cell system consisting of a glass optical pumping cell located outside the scattering chamber and coupled through a narrow transition tube to the target cell. The operating pressure of the helium gas was 2 Torr. Two 3.8 cm diameter, 5.1 cm long cylindrical Pyrex pumping cells were constructed for the target: one for producing polarizations in the horizontal plane (the  $\hat{x}$ - $\hat{z}$  plane) and a second for vertical ( $\hat{y}$ ) polarizations. The polarized gas from the pumping cell diffused down into the scattering cell through a 4.8-mm-i.d. brass transition tube. The cylindrical scattering cell was machined from copper and had a height of 31.8 mm and a diameter of 57.2 mm. The left and right side windows were constructed so that the detectors could view a continuous range of lab angles from  $37.5^\circ$  to  $147.5^\circ$ . The beam entrance and exit foils were 2.54  $\mu\text{m}$  thick molybdenum foil, while the side windows were covered with 25.4  $\mu\text{m}$  kapton foil. The scattering cell was cooled by a cold finger connection to a liquid nitrogen Dewar. The base temperature of the scattering cell during data acquisition was typically 125 K.

During operation the polarization of the helium in the pumping cell was monitored by measuring the optical po-

larization of the discharge light. It is well known that the degree of circular polarization from the  $3^1D \rightarrow 2^1P$  electronic transition at 667.8 nm can be related to the ground state  $^3\text{He}$  nuclear polarization [19–21]. The circular polarization of the light from the discharge was monitored with an optical polarimeter located along the axis of the pumping cell. The polarimeter operated by using a rotating quarter-wave plate to transform the incoming circularly polarized light into rotating, linearly polarized light. This linearly polarized light then passed through a fixed linear polarizer, to produce a sinusoidally varying signal with an amplitude proportional to the original circular polarization. The light intensity was measured with a photomultiplier tube and the resulting signals were sent to a computer, where they were analyzed and stored for future data reduction. In Sec. IV D 3 we will discuss how the nuclear polarization in the scattering cell was determined for the final analysis.

Helmholtz coils surrounding the entire scattering chamber were used to provide a uniform guide field of typically 2.5 mT. The coils can be mounted to produce a magnetic field along any of the three orthogonal coordinate axes.

### B. The polarized beam

In order to measure all of the spin observables in Eq. (2), it is necessary to produce proton beams polarized along the  $\hat{x}$  and  $\hat{z}$  directions as well as along  $\hat{y}$ . As described in Sec. III A, the spin orientation of the beam was set using a Wien filter. The polarimeter described in Sec. III A was originally designed to measure only the  $\hat{y}$  component of the beam polarization. To measure the  $\hat{x}$  component, a flange was constructed to rotate the entire polarimeter assembly by  $90^\circ$ . An equivalent arrangement is not possible for polarizations along the  $\hat{z}$  axis, and so the procedure used was to alternate between runs with  $\hat{x}$  and  $\hat{z}$  polarizations. The polarization for a given  $\hat{z}$  run was taken as the average of the  $\hat{x}$  runs that preceded and followed it. The typical polarization variance between successive  $\hat{x}$  runs was 1%.

### C. Data acquisition

Protons from  $p$ - $^3\text{He}$  elastic scattering in the target cell were detected with silicon surface barrier detectors. The scattering volume for each detector was defined by a slit system consisting of two pairs of stainless steel slits sep-

arated by 7.62 cm. The front and back slit apertures were both 2 mm wide, producing an angular acceptance of  $\pm 1.5^\circ$ . During data acquisition, measurements were taken at five different angles simultaneously, with pairs of detectors at symmetric angles to the left and right of the beam.

Extraction of the spin-correlation coefficients requires a relative measurement of the integrated charge for the various spin states. This was accomplished with a Faraday cup located behind the polarimeter.

The polarized target data were taken in a series of runs in which the target was configured for polarization along the  $\hat{x}$ ,  $\hat{y}$ , or  $\hat{z}$  direction. During the data acquisition, the target spin was flipped every 10 min. The proton analyzing power  $A_{y0}$ , helium analyzing power  $A_{0y}$ , and spin correlation coefficient  $A_{yy}$  were all measured simultaneously with beam and target polarized along the  $y$  axis. The remaining spin correlation coefficients  $A_{xx}$ ,  $A_{zz}$ ,  $A_{zx}$ , and  $A_{zz}$  were measured individually in runs with beam and target polarized along  $\hat{x}$  or  $\hat{z}$ . The measurements were taken in a series of 2 h runs in order to minimize the possibility of data loss due to equipment failure. It was typically necessary to perform eight to ten 2 h runs in order to reach the desired statistical accuracy.

Measurements of the quantities  $A_{y0}$ ,  $A_{0y}$ , and  $A_{yy}$  were obtained at 8 angles at the energy of 4.01 MeV. At each of the four remaining energies, 5.54, 7.03, 8.52, and 10.01 MeV, the measurements were taken at 10 angles. The remaining second-order polarization observables,  $A_{xx}$ ,  $A_{zz}$ ,  $A_{zx}$ , and  $A_{zz}$ , were measured at 5 angles at the single energy of 5.54 MeV.

### D. Data reduction

#### 1. Extraction of the observables

For an experiment involving both a polarized beam and target, the extraction of first- and second-order polarization observables is complicated due to the large number of terms in the differential cross section. Following the development of Vigdor *et al.* [22], we write the cross sections of Eq. (2), as sums and/or differences of eight separate terms which are distinguished by their symmetry behavior under three different operations: interchange of left and right detectors, spin reversal of the proton, and spin reversal of the  $^3\text{He}$  nucleus. These eight quantities, denoted as  $A_i$  and  $B_i$  for  $i = 1, 4$  are listed in Table II, along with their symmetry properties un-

TABLE II. The eight independent parts of the polarized differential cross section. Each term has a unique symmetry under interchange of left and right detectors, proton spin reversal, and  $^3\text{He}$  spin reversal. The notation is explained in the text. This table is based on the development of Vigdor *et al.* [22].

| $l \leftrightarrow r$ | Symmetry under     |                      | Expression for the ratio of polarized to unpolarized cross section   |
|-----------------------|--------------------|----------------------|--|
|                       | Beam spin reversal | Target spin reversal |  |
| +                     | +                  | +                    | $A_0 = 1 + \bar{P}_{by}\bar{P}_{ty}A_{yy} + \bar{P}_{bx}\bar{P}_{tx}A_{xx} + \bar{P}_{bz}\bar{P}_{tz}A_{zz}$ |
| +                     | -                  | +                    | $A_1 = P_{by}\bar{P}_{ty}A_{yy} + P_{bx}\bar{P}_{tx}A_{xx} + P_{bz}\bar{P}_{tz}A_{zz}$                       |
| +                     | +                  | -                    | $A_2 = \bar{P}_{by}P_{ty}A_{yy} + \bar{P}_{bx}P_{tx}A_{xx} + \bar{P}_{bz}P_{tz}A_{zz}$                       |
| +                     | -                  | -                    | $A_3 = P_{by}P_{ty}A_{yy} + P_{bx}P_{tx}A_{xx} + P_{bz}P_{tz}A_{zz}$   |
| -                     | +                  | +                    | $B_0 = \bar{P}_{by}A_{y0} + \bar{P}_{ty}A_{0y} + \bar{P}_{bx}P_{tx}A_{xx} + \bar{P}_{bz}\bar{P}_{tz}A_{zz}$  |
| -                     | -                  | +                    | $B_1 = P_{by}A_{y0} + P_{ty}A_{0y} + P_{bx}\bar{P}_{tx}A_{xx} + P_{bz}\bar{P}_{tz}A_{zz}$                    |
| -                     | +                  | -                    | $B_2 = P_{ty}A_{0y} + \bar{P}_{by}P_{tx}A_{xx} + \bar{P}_{bz}P_{tz}A_{zz}$                                   |
| -                     | -                  | -                    | $B_3 = P_{bx}P_{tx}A_{xx} + P_{bz}P_{tz}A_{zz}$  |

der the aforementioned operations. In these expressions, the quantities  $P_b$  and  $P_t$  refer to the average polarization magnitudes (typically 0.85 for the beam and 0.30 for the target), while  $\bar{P}_{b(t)}$  represent the differences in the polarization magnitudes between the + and - spin states ( $\bar{P} \simeq 0$ ).

For any given measurement it is useful to distinguish between the primary and secondary polarization axes. The primary axis is the direction along which the polarization vector needs to be oriented in order to measure the desired observable. The secondary axes are those directions not involved in the measurement. For example, to measure  $A_{xz}$ , the primary polarization axes are  $\hat{x}$  and  $\hat{z}$  for the beam and target respectively, while the secondary axes are  $\hat{y}$  and  $\hat{z}$  for the beam and  $\hat{y}$  and  $\hat{x}$  for the target. The main point is to realize that in any given measurement the secondary  $P_t$  and  $P_b$  polarization parameters as well as all of the  $\bar{P}_t$  and  $\bar{P}_b$  polarizations are small (for our experiment the maximum values of  $\bar{P}_b$  and  $\bar{P}_t$  were 0.01 and 0.02, respectively, while the secondary polarizations had extreme values of  $P_b = 0.03$  and  $P_t = 0.01$ ).

The procedure we use to determine the analyzing powers and spin-correlation coefficients is as follows. The first-order analyzing powers  $A_{y0}$  and  $A_{0y}$  are extracted from  $B_1$  and  $B_2$  respectively. The quantities  $A_{xx}$ ,  $A_{yy}$ , and  $A_{zz}$  are all determined by extracting the value of  $A_3$  (for runs with different spin orientations). Similarly  $A_{xz}$  and  $A_{zx}$  are both determined from extracted values of  $B_3$ . Inspection of the expressions in Table II shows that in all cases the term of interest in  $A_3$ ,  $B_1$ ,  $B_2$ , or  $B_3$  is associated with unwanted terms, but that these unwanted terms always involve a product of two small polarization parameters. These contaminant terms are typically an order of magnitude smaller than the ultimate statistical errors, and consequently were neglected in the analysis.

The individual  $A_i$  and  $B_i$  terms are extracted as follows. The counts obtained in the right and left detectors are denoted as  $R_{ij}$  and  $L_{ij}$ , respectively, where the index  $i$  refers to the proton spin state and the index  $j$  refers to the  $^3\text{He}$  spin state. (Both indices can assume values of + or -, depending on whether the spin state is parallel or antiparallel to the polarization axis.) Similarly,  $I_{ij}$  represents the integrated charge, where the indices have the same meaning as above. Using these quantities, the sums and differences  $S_{ij}$  and  $D_{ij}$  are defined according to

$$S_{ij} = \frac{L_{ij} + R_{ij}}{I_{ij}}, \quad (5)$$

$$D_{ij} = \frac{L_{ij} - R_{ij}}{I_{ij}}. \quad (6)$$

We now construct the following four pairs of sums:

$$S_0 \equiv S_{++} + S_{+-} + S_{-+} + S_{--}, \quad (7)$$

$$D_0 \equiv D_{++} + D_{+-} + D_{-+} + D_{--}, \quad (7)$$

$$S_1 \equiv S_{++} + S_{+-} - S_{-+} - S_{--}, \quad (8)$$

$$D_1 \equiv D_{++} + D_{+-} - D_{-+} - D_{--}, \quad (8)$$

$$S_2 \equiv S_{++} - S_{+-} + S_{-+} - S_{--}, \quad (9)$$

$$D_2 \equiv D_{++} - D_{+-} + D_{-+} - D_{--}, \quad (9)$$

$$S_3 \equiv S_{++} - S_{+-} - S_{-+} + S_{--}, \quad (10)$$

$$D_3 \equiv D_{++} - D_{+-} - D_{-+} + D_{--}. \quad (10)$$

With these definitions, it can easily be shown that the  $A_i$  and  $B_i$  terms (and hence the observables themselves) are given by

$$A_i = (S_i S_0 - D_i D_0) / \left( (S_0)^2 - (D_0)^2 \right), \quad (11)$$

$$B_i = (D_i S_0 - S_i D_0) / \left( (S_0)^2 - (D_0)^2 \right), \quad (12)$$

where we have again neglected terms that are second order in the small polarization parameters.

The method presented here for obtaining the spin observables assumes that the relative integrated charges  $I_{ij}$  can be well determined. The measurement of these quantities is potentially a serious problem because the Faraday cup we use is located in the helium gas that fills the polarimeter (so in reality the cup functions like a low-voltage ionization chamber). From studies of the long-term stability of the readings we believe that variations in the collection efficiency are no greater than  $\pm 5\%$  over the 10 min target spin flip period. Assuming that the efficiency variations occur randomly (i.e., that they are not correlated with spin flips) one can show that the resulting systematic errors are negligible.

## 2. Background removal

In general, the observed proton spectra were reasonably clean, consisting of a single strong peak from elastic scattering along with a smoothly varying low energy background. This background, which was strongest at the most forward and most backward angles, probably results from beam particles which scatter in the cell entrance foil and then strike parts of the cell which are viewed by the detectors. Peaks from foil-foil scattering were present at the most forward angles, but in all cases these peaks were well separated from the elastically scattered proton.

Figure 1 shows a proton spectrum obtained at  $E_p = 7.03$  MeV and  $\theta_{\text{lab}} = 37.5^\circ$ , the most forward angle at

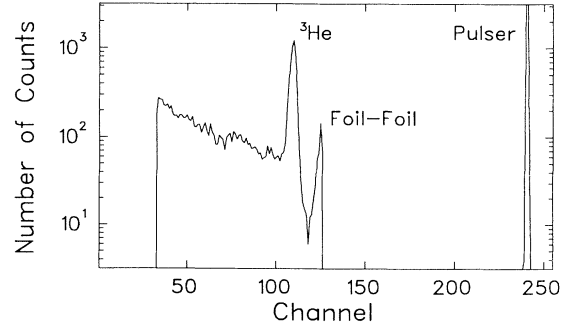


FIG. 1. Pulse height spectrum for  $E_p = 7.03$  MeV and  $\theta_{c.m.} = 49.3^\circ$ . The three peaks, in order from left to right, correspond to protons scattered from  $^3\text{He}$ , protons from foil-foil scattering, and pulser counts. The spectrum shown is an example of the most severe case of background contamination encountered in the experiment.

which data were taken. The spectrum shown is for the right detector and the  $-$  spin state, with beam and target both polarized along the  $\hat{y}$  axis. This spectrum represents the most severe case of background contamination observed in the experiment.

Background subtraction was accomplished with the aid of a peak-fitting program. The proton elastic scattering peak was modeled using a split, hyper-Gaussian function, and the background was assumed to be linear. Not all of the fit parameters were needed for every angle and energy, and in some cases, particularly for lab angles around  $90^\circ$ , the background was non-existent. However, in order to ensure consistency in the data reduction a computer program was written to automate the process whether or not background subtraction was necessary.

The success of the background subtraction scheme was tested by subjecting the data to a "channel-by-channel" analysis. The procedure is illustrated in Fig. 2. Here the upper panel shows an expanded version of the raw data from Fig. 1 (solid points), along with the fit (solid curve) and the resulting background subtracted spectrum (open points). The lower panel shows a channel by channel calculation of the proton analyzing power  $A_{y0}$  obtained from the displayed spectrum together with analogous spectra for the other spin states and for the left detector. Notice that when the unsubtracted spectra are used (solid

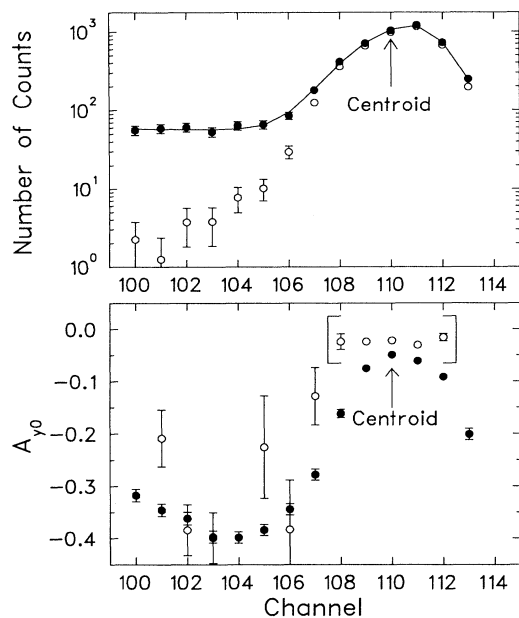


FIG. 2. Results of a channel by channel analysis. The solid points in the upper panel show an expanded version of the elastic proton peak from Fig. 1. The curve is the fit to these data obtained with a peak fitting algorithm, and the open points show the resulting background-subtracted spectrum. The lower panel shows the values of the analyzing power,  $A_{y0}$ , extracted channel by channel from the spectra shown above. The solid points correspond to the raw unsubtracted data, while the open circles correspond to the background-subtracted results. The points within the brackets were used to determine the final value of  $A_{y0}$ .

points) the  $A_{y0}$  values vary across the peak, indicating the presence of a background whose analyzing power differs from that of the peak. However, the subtracted spectra show the expected behavior for a background-free peak, namely an analyzing power which is independent of position across the peak. The final result for the value of  $A_{y0}$  in this example was taken to be the weighted mean of the points shown within the brackets. In most cases the effect of the background subtraction was far less extreme than the example shown.

The effectiveness of the background subtraction algorithm may also be judged by comparing the final proton analyzing powers with the results obtained from the unpolarized target experiment (in which the backgrounds were negligible). Overall the agreement of the two data sets is excellent. When both data sets are simultaneously included in a global phase shift fit (Ref. [23]), we obtain a reduced  $\chi^2_\nu$  of 0.96 for the unpolarized target data, and 0.87 for the polarized data.

### 3. Target polarization determination

In extracting the target analyzing power and spin correlation parameters, care must be taken to correctly determine the polarization in the scattering cell. This is a complicated task, due to the fact that the scattering cell polarization is never measured directly. The standard approach for determining this polarization involves a two step process. The nuclear polarization in the pumping cell is first determined by measuring the circular polarization,  $P_\odot$ , of the 668 nm light from the discharge. Recent work on calibrating the conversion factor between  $P_\odot$  and the nuclear polarization has led to results which are typically accurate to  $\pm 2\%$  [20, 21]. The second step in the process is to then convert the pumping cell polarization into a scattering cell polarization by using measurements of the mixing ratio between the two cells (see, for example, Ref. [24]). The determination of this mixing ratio is not simple. The usual approach is to determine various diffusion and relaxation rates of the double cell system, but since this method is rather indirect the determination of the scattering cell polarization  $P_t$  is subject to substantial errors.

We have chosen to adopt a different procedure for determining the scattering cell polarization. Basically, this method involves normalizing the observed target analyzing powers to predictions obtained from a global phase shift fit of the previously existing  $p$ - $^3\text{He}$  scattering data [23]. In detail, the procedure we used is as follows. Our new polarized target data set consists of 48 2 h runs in the energy range 7–10 MeV in which the beam and target were polarized along the  $\hat{y}$  axis. For each of these runs there are measurements of the target asymmetry,  $P_t A_{0y}$ , at 5 c.m. angles. For each run  $i$  (where  $i = 1, 48$ ) we determine the optimum value of  $P_t$  by normalizing the measured target asymmetries to the  $A_{0y}$  phase shift predictions. The best-fit value of  $P_t$  and the measured value of the 668 nm circular polarization,  $P_\odot$ , for each run are then combined to obtain a value of the ratio

$$R = P_t/P_\odot. \quad (13)$$

TABLE III. Measurements of the proton analyzing power  $A_{y0}$  obtained with the polarized  $^3\text{He}$  target. In addition to the quoted errors, the measurements are subject to an overall scale factor uncertainty of 2% for  $E_p < 8$  MeV and 1% for  $E_p > 8$  MeV.

| $\theta_{\text{c.m.}}$ | 4.01 MeV   | 5.54 MeV    | 7.03 MeV    | 8.52 MeV    | 10.01 MeV   |
|------------------------|------------|-------------|-------------|-------------|-------------|
| 49.3°                  | 0.1233(27) | 0.0316(13)  | -0.0238(20) | -0.0527(17) | -0.0733(21) |
| 61.8°                  | 0.1671(50) | 0.0403(47)  | -0.0289(30) | -0.0745(22) | -0.1014(23) |
| 73.9°                  | 0.2468(44) | 0.1033(25)  | -0.0033(32) | -0.0799(31) | -0.1205(35) |
| 85.6°                  | 0.3487(71) | 0.2249(62)  | 0.0809(40)  | -0.0297(42) | -0.0985(43) |
| 96.6°                  | 0.3994(55) | 0.3948(47)  | 0.2718(69)  | 0.1347(68)  | 0.0121(85)  |
| 107.1°                 | 0.3685(79) | 0.4880(111) | 0.5084(86)  | 0.4571(93)  | 0.3480(95)  |
| 116.9°                 | 0.3011(65) | 0.4452(47)  | 0.5321(77)  | 0.5794(92)  | 0.6239(152) |
| 126.1°                 | 0.2322(80) | 0.3404(76)  | 0.4246(64)  | 0.4950(80)  | 0.5578(87)  |
| 142.9°                 | —          | 0.1943(35)  | 0.2343(62)  | 0.2714(61)  | 0.2820(87)  |
| 150.6°                 | —          | 0.1312(62)  | 0.1633(44)  | 0.1904(47)  | 0.2115(54)  |

TABLE IV. Measurements of the target analyzing power  $A_{0y}$ . In addition to the quoted errors, the measurements are subject to an overall scale factor uncertainty of  ${}_{-10}^{+3}\%$  (see Sec. IV D 3).

| $\theta_{\text{c.m.}}$ | 4.01 MeV    | 5.54 MeV     | 7.03 MeV     | 8.52 MeV     | 10.01 MeV    |
|------------------------|-------------|--------------|--------------|--------------|--------------|
| 49.3°                  | 0.0205(73)  | -0.0055(38)  | -0.0270(72)  | -0.0580(56)  | -0.0678(67)  |
| 61.8°                  | 0.0531(126) | -0.0056(103) | -0.0452(58)  | -0.0740(64)  | -0.0752(65)  |
| 73.9°                  | 0.0571(102) | 0.0051(66)   | -0.0354(113) | -0.0748(104) | -0.0831(110) |
| 85.6°                  | 0.0806(195) | 0.0589(174)  | -0.0264(109) | -0.0748(137) | -0.0998(123) |
| 96.6°                  | 0.1070(154) | 0.1004(133)  | 0.0630(230)  | -0.0090(206) | -0.0650(329) |
| 107.1°                 | 0.1022(301) | 0.1553(286)  | 0.1264(194)  | 0.1061(234)  | 0.0607(245)  |
| 116.9°                 | 0.0837(173) | 0.1356(132)  | 0.1684(241)  | 0.1863(328)  | 0.1510(431)  |
| 126.1°                 | 0.0730(243) | 0.1167(245)  | 0.1472(165)  | 0.1802(209)  | 0.1636(227)  |
| 142.9°                 | —           | 0.0552(103)  | 0.0838(249)  | 0.0824(198)  | 0.0905(299)  |
| 150.6°                 | —           | 0.0517(250)  | 0.0562(140)  | 0.0671(132)  | 0.0627(147)  |

TABLE V. Measurements of the spin correlation coefficient  $A_{yy}$ . In addition to the quoted errors, the measurements are subject to an overall scale factor uncertainty of  ${}_{-10}^{+3}\%$  (see Sec. IV D 3).

| $\theta_{\text{c.m.}}$ | 4.01 MeV    | 5.54 MeV    | 7.03 MeV    | 8.52 MeV    | 10.01 MeV    |
|------------------------|-------------|-------------|-------------|-------------|--------------|
| 49.3°                  | 0.1101(87)  | 0.1424(47)  | 0.1424(82)  | 0.1671(66)  | 0.1751(80)   |
| 61.8°                  | 0.1153(170) | 0.1360(124) | 0.1409(100) | 0.1679(81)  | 0.1447(78)   |
| 73.9°                  | 0.0626(122) | 0.1062(78)  | 0.1295(129) | 0.1542(122) | 0.1161(166)  |
| 85.6°                  | 0.0509(245) | 0.0996(238) | 0.1023(128) | 0.0949(152) | 0.0971(146)  |
| 96.6°                  | 0.0488(169) | 0.0323(157) | 0.0412(275) | 0.0546(242) | 0.0801(389)  |
| 107.1°                 | 0.0219(303) | 0.0216(358) | 0.0038(227) | 0.0004(264) | -0.0239(292) |
| 116.9°                 | 0.0278(205) | 0.0660(156) | 0.0115(287) | 0.0295(386) | -0.0202(510) |
| 126.1°                 | 0.0568(293) | 0.0835(311) | 0.0562(194) | 0.0359(257) | 0.0314(271)  |
| 142.9°                 | —           | 0.0972(122) | 0.0878(247) | 0.0706(268) | 0.0498(280)  |
| 150.6°                 | —           | 0.1060(294) | 0.0927(139) | 0.0727(153) | 0.0622(200)  |

TABLE VI. Measurements of the spin correlation coefficients  $A_{xz}$ ,  $A_{zx}$ ,  $A_{xx}$ , and  $A_{zz}$  at 5.54 MeV. In addition to the quoted errors, the measurements are subject to an overall scale factor uncertainty of  ${}_{-10}^{+3}\%$  (see Sec. IV D 3).

| $\theta_{\text{c.m.}}$ | $A_{xz}$     | $A_{zx}$     | $A_{xx}$    | $A_{zz}$     |
|------------------------|--------------|--------------|-------------|--------------|
| 49.3°                  | 0.0577(152)  | 0.0532(53)   | 0.1142(51)  | 0.1612(143)  |
| 73.9°                  | 0.1197(202)  | 0.1052(90)   | 0.0636(90)  | 0.0684(216)  |
| 96.6°                  | 0.0454(339)  | 0.1004(167)  | 0.0068(146) | -0.1886(390) |
| 116.9°                 | -0.1541(352) | -0.0255(176) | 0.0140(162) | -0.0562(392) |
| 142.9°                 | -0.0878(241) | -0.0299(126) | 0.0637(117) | 0.1414(268)  |

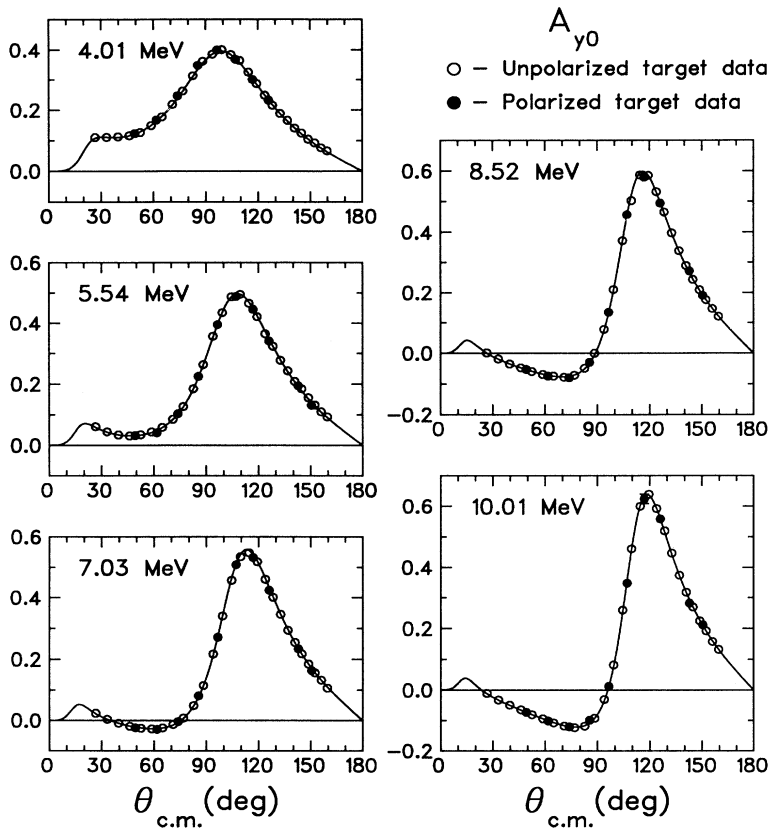


FIG. 3. Measurements of the proton analyzing power  $A_{y0}$ . In all cases the error bars are smaller than the plotting symbols. The curves are the results of an effective range analysis discussed in the accompanying paper [23].

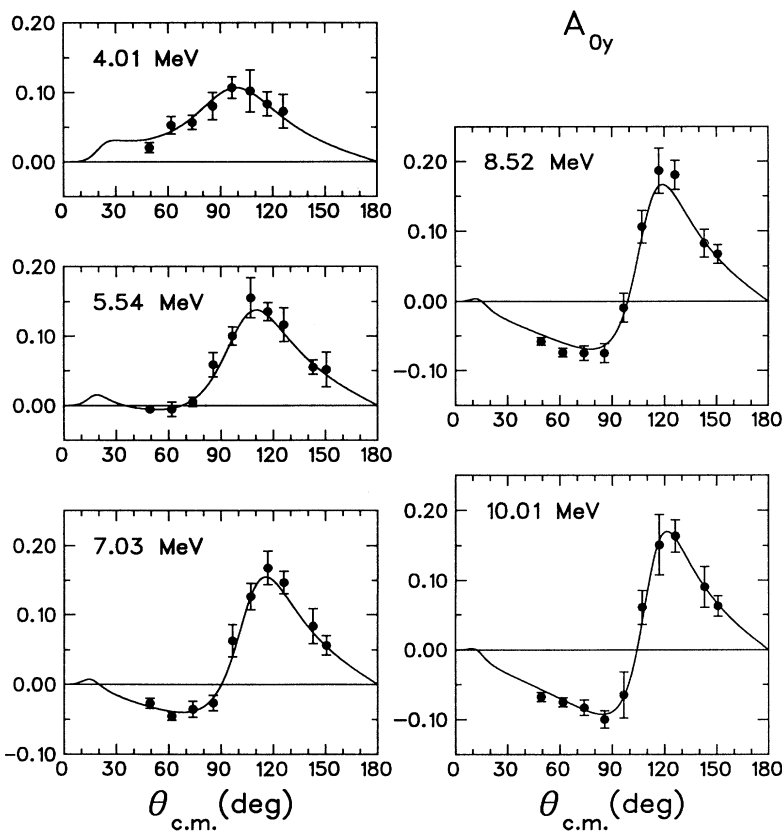


FIG. 4. Measurements of the  $^3\text{He}$  analyzing power  $A_{0y}$ . The curves are the results of an effective range analysis discussed in the accompanying paper [23].

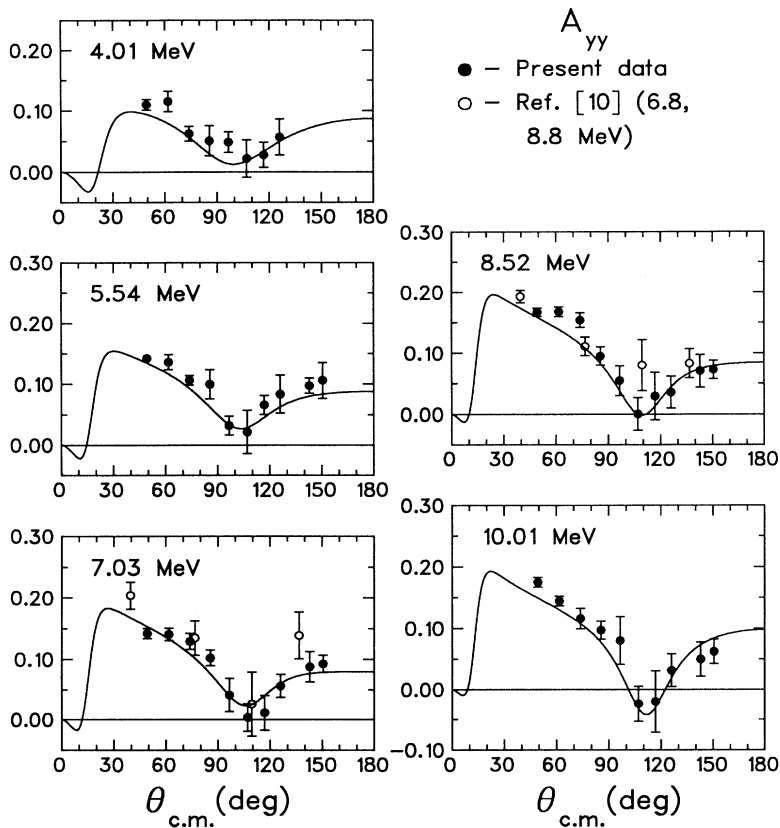


FIG. 5. Measurements of the spin correlation coefficient  $A_{yy}$ . The open circles are data from May *et al.* at 6.8 and 8.8 MeV [10]. The curves are the results of an effective range analysis discussed in the accompanying paper [23].

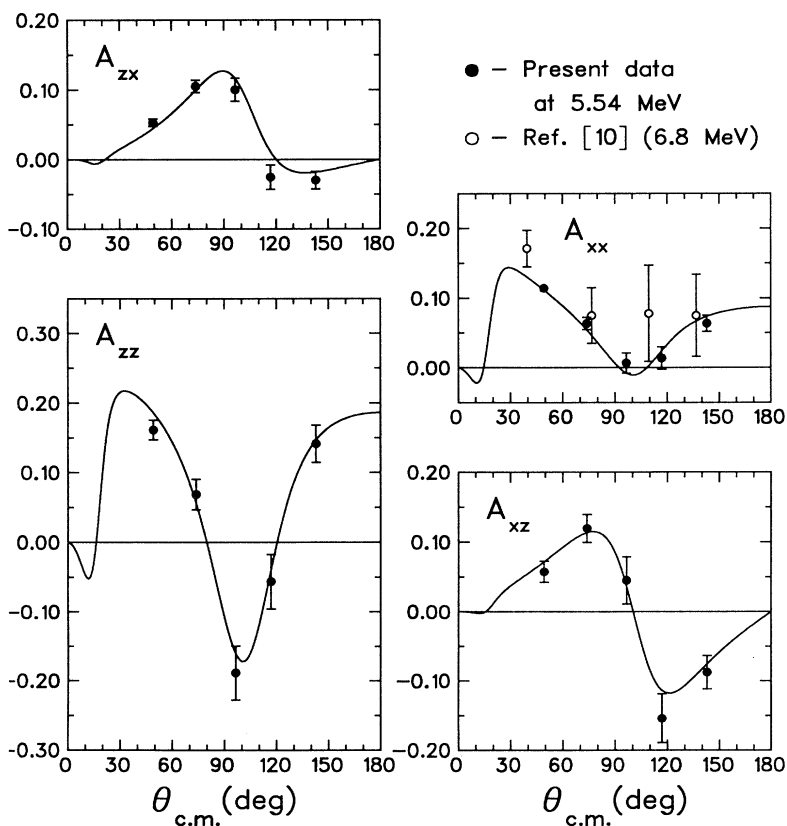


FIG. 6. Measurements of the spin correlation coefficients  $A_{zx}$ ,  $A_{zz}$ ,  $A_{xx}$ , and  $A_{xz}$  at 5.54 MeV. The open circles are data from May *et al.* at 6.8 MeV [10]. The curves are the results of an effective range analysis discussed in the accompanying paper [23].

Finally, an overall optimum value of  $R$  is found by taking a weighted average of the 48 separate determinations. The result we obtain is

$$\bar{R} = 11.86 \pm 0.25, \quad (14)$$

where the error represents only the statistical uncertainty in the final value of  $\bar{R}$ .

Having chosen a value of  $\bar{R}$  we were then able to carry out the actual data analysis. For any given run (no matter what the target configuration) the target polarization was determined using the recorded optical polarization for that run:

$$P_t = \bar{R}P_\odot. \quad (15)$$

The target polarizations thus determined are subject to two sources of error, a random error arising from statistical fluctuations in the measurement of  $P_\odot$  (typically on the order of  $\pm 3\%$ ) and an overall normalization error (discussed further below) arising from the uncertainty in the value of  $\bar{R}$ .

There are a number of factors that need to be taken into account in estimating the scale factor uncertainty. One important question concerns the extent to which previous polarized target measurements can skew the phase shift predictions on which we base our determination of  $\bar{R}$ . The database that was used in the phase shift fits contained 105 previous measurements of  $A_{0y}$ , obtained from three different institutions, in the energy range 2.3–12.4 MeV. We find that if the normalization of these data is changed over the range  $-2\%$  to  $+12\%$ , the quality of the phase shift fit does not deteriorate, and the extracted values of  $\bar{R}$  essentially track with the normalization change (i.e.,  $\bar{R}$  varies over the range  $+2\%$  to  $-12\%$ ). Thus, in effect, the procedure we use ties the normalization of our data to that of the previous measurements. The previous measurements were all obtained with single-cell targets, so that determination of the polarization mixing ratio was not an issue, but these measurements are still subject to normalization uncertainties, probably on the order of 5–10%.

It is also informative to compare our value of  $\bar{R}$  with results obtained by combining measurements of the 668 nm optical-to-nuclear conversion factor with determinations of the polarization mixing ratio. If we take the mixing ratio to be 1, the measured 668 nm conversion factors (at  $P = 2$  Torr) from Refs. [19–21] give  $R$  values of 11.7, 10.1, and 10.5, respectively, where the Ref. [21] result was obtained by linear interpolation of the measurements at 1.6 and 3.0 Torr. The last two determinations are claimed to be accurate to 2–3%.

The final piece of information we use in assessing the normalization uncertainty of our measurements is obtained by including the new measurements in the global phase shift analysis described in the accompanying paper [23]. With the new target analyzing power and spin-

correlation data included, we find that the overall best fit is obtained if the value of  $\bar{R}$  is renormalized by  $-4 \pm 3\%$ .

All of these results taken together suggest a probable systematic error on the order of 5–10%. Furthermore, the preponderance of evidence points in the direction of smaller  $\bar{R}$  values, and consequently we take the normalization uncertainty to be  ${}^{+3}_{-10}\%$ .

## E. Results

The results obtained from the experiments with the polarized  $^3\text{He}$  target are listed in Tables III–VI. The quoted errors are dominated by counting statistics, but include as well the statistical errors in the determination of the beam and target polarizations. Possible systematic errors resulting from the choice of background subtraction algorithm are thought to be negligible, and were taken to be zero. For the polarized target measurements the uncertainty in the beam energy is  $\pm 0.02$  MeV and the angle uncertainty is  $\pm 0.05^\circ$ . The overall normalization errors resulting from the beam and target polarization measurements are not included in the quoted uncertainties.

## V. SUMMARY AND CONCLUSIONS

We have obtained new measurements of the analyzing powers and spin-correlation parameters for  $p$ - $^3\text{He}$  elastic scattering between 4 and 10 MeV. The measurements of the proton analyzing power  $A_{y0}$  are shown in Fig. 3. Note that the measurements obtained with the polarized target are in good agreement with the unpolarized target data. Figure 4 shows our results for the target analyzing power, while the measurements of the spin correlation coefficients are given in Figs. 5 and 6. For comparison, Figs. 5 and 6 also show the measurements of May and Baker at 6.8 and 8.8 MeV [10]. The agreement between our data and the previous work is quite good.

Also shown in each figure are the results obtained from an effective-range phase shift analysis of most of the available  $^3\text{He}(p,p)^3\text{He}$  data over the energy range of 0 to 12 MeV. This analysis, which is described in detail in the following paper [23], included a total of 1085 measurements of which 299 were from the present experiment. Up until the present time, the determination of a unique phase shift set in this energy range had not been possible due to the lack of spin correlation data [3, 25].

## ACKNOWLEDGMENTS

The authors are grateful to the students and staff of Wisconsin nuclear physics group for their assistance with the data acquisition and the polarized target development. This work was supported by the National Science Foundation Grant No. PHY-9019983.

- [1] T. A. Tombrello, *Phys. Rev.* **138**, B40 (1965).
- [2] L. W. Morrow and W. Haeberli, *Nucl. Phys.* **A126**, 225 (1969).
- [3] G. Szaloky and F. Seiler, *Nucl. Phys.* **A303**, 57 (1978).
- [4] P. Heiss and H. H. Hackenbroich, *Nucl. Phys.* **A182**, 522 (1972).
- [5] G. M. Hale, J. J. Devaney, D. C. Dodder, and K. Witte, *Bull. Am. Phys. Soc.* **19**, 506 (1974).
- [6] H. Furutani, H. Horiuchi, and R. Tamagaki, *Prog. Theor. Phys.* **62**, 981 (1979).
- [7] L. Beltramin, R. Del Frate, and G. Pisent, *Nucl. Phys.* **A442**, 266 (1985).
- [8] G. R. Plattner, M. Bornand, and R. D. Viollier, *Phys. Rev. Lett.* **39**, 127 (1977).
- [9] D. H. McSherry and S. D. Baker, *Phys. Rev. C* **1**, 888 (1970).
- [10] D. P. May, S. D. Baker, G. G. Ohlsen, and R. G. Hard-ekopf, *Bull. Am. Phys. Soc.* **18**, 1395 (1973).
- [11] P. La France and P. Winternitz, *J. Phys. (Paris)* **41**, 1391 (1980).
- [12] W. Haeberli *et al.*, *Nucl. Instrum. Methods.* **196**, 319 (1982).
- [13] P. Schwandt, T. Clegg, and W. Haeberli, *Nucl. Phys.* **A163**, 432 (1971).
- [14] P. C. Colby, Ph.D. thesis, University of Wisconsin-Madison (1984).
- [15] R. G. Milner, R. D. McKeown, and C. E. Woodward, *Nucl. Instrum. Methods.* **A274**, 56 (1989).
- [16] F. D. Colegrove, L. D. Scheerer, and G. K. Walters, *Phys. Rev.* **132**, 2561 (1963).
- [17] L. D. Scheerer, M. Leduc, D. Vivien, A. M. Lejus, and J. Thery, *IEEE Quantum Electron.* **QE-22**, 713 (1986).
- [18] M. T. Alley, Ph.D. thesis, University of Wisconsin-Madison (1992).
- [19] M. Pinard and J. Van Der Linde, *Can. J. Phys.* **52**, 1615 (1974).
- [20] W. Lorenzon, T. R. Gentile, H. Gao, and R. D. McKeown, *Phys. Rev. A* **47**, 468 (1993).
- [21] N. Bigelow, P. J. Nacher, and M. Leduc, *J. Phys. II (Paris)* **2** 2159 (1992).
- [22] S. E. Vigdor *et al.*, *Phys. Rev. C* **46**, 410 (1992).
- [23] M. T. Alley and L. D. Knutson, *Phys. Rev. C* **48**, 1901 (1993), the following paper.
- [24] C. E. Jones, Ph.D. thesis, California Institute of Technology (1992).
- [25] C. O. Blyth, O. Karban, W. B. Powell, and S. Roman, *Nucl. Phys.* **A247**, 1 (1975).